Molecular dynamics simulation of a smectic liquid crystal with atomic detail

Egberts, E.; Berendsen, H. J. C.

Published in:
Journal of Chemical Physics

DOI:
10.1063/1.454893

Publication date:
1988

Molecular dynamics simulation of a smectic liquid crystal with atomic detail

E. Egberts, and H. J. C. Berendsen

Citation: The Journal of Chemical Physics **89**, 3718 (1988); doi: 10.1063/1.454893
View online: https://doi.org/10.1063/1.454893
View Table of Contents: http://aip.scitation.org/toc/jcp/89/6
Published by the American Institute of Physics

Molecular dynamics simulation of a smectic liquid crystal with atomic detail

E. Egberts and H. J. C. Berendsen[a)]
Laboratory of Physical Chemistry, University of Groningen, Nyenborgh 16, 9747 AG Groningen, The Netherlands

(Received 12 November 1987; accepted 31 May 1988)

A molecular dynamics simulation of a sodium–decanoate/decanol/water system is reported. The system is treated in full atomic detail, with the exception of CH_2 and CH_3 groups that are considered to be "united atoms," and is a refinement of a previous model membrane [Mol. Phys. **11**, 1 (1983)]. The long-range Coulomb interactions were included specifically. The order parameters of the chain units of the lipids and diffusion constants of components in the system calculated from the simulation agree well with those reported in experiments on this model membrane. The overall structure of the membrane shows considerable disorder, with a broad lipid–water interface, extending over approximately 1 nm. The distribution of the components is such that an almost complete charge cancellation occurs throughout the system, which is in contradiction with the generally assumed electrical double layer structure for membranes. A counterion condensation of 70% is observed. Both the translational and the rotational motions of water are slowed down compared to bulk water. The penetration of water into the hydrocarbon region of the membrane is substantial. Pair correlations of various atom pairs, and dihedral statistics and transition rates of the dihedrals in the lipids are reported. The distributions of chain segments of the lipids, of water molecules, and of sodium ions are compared with theoretical predictions.

I. INTRODUCTION

The smectic liquid crystalline state is one of the important aggregation states of binary or ternary mixtures containing amphiphilic molecules. Its structure can be characterized as a multilamellar aggregate built up from bilayers similar to the bilayers in lipid membranes. The biological interest in such membranes has considerably stimulated experimental and theoretical research in this field. The recent advance in computer simulation methods now enables us to describe the dynamic and static properties of the lipid matrix in terms of the fundamental interactions between the molecules involved.

Theoretical work on lipid bilayers has covered potentials of mean force and specific defect structures. We mention some approaches: Nagle[1,2] performed free energy calculations, using statistical mechanics, for the description of the behavior of lipid bilayers near the gel to liquid crystal phase transition, from which he concluded that this transition depends sensitively on even quite small headgroup interactions. A similar method was followed by Wiegel,[3] who constructed a two-dimensional lattice model for lipid monolayers, that are considered to bear much resemblance to layers in a bilayer structure. In the statistical mechanical work by Jähnig,[4] the lipid membrane is approximated by a layer of identical polymethylene chains, with one end attached to a surface plane. This model has much in common with the work of Marcelja,[5] but is analytically solvable due to the treatment of the chains as continuous elastic lines. Both authors discuss lipid structure in terms of orientational order parameters. Gruen[6] presented a simple model for the state of chains in amphiphilic aggregates, by the generation of all possible internal bond sequences of a single chain. His model for bilayers distinguishes between hydrocarbon core, headgroup region, and water layer, and provides a good model system for comparison with static properties derived from molecular dynamics simulations of bilayers. Leermakers *et al.*[7] extended a lattice theory for the formulation of the formation and properties of amphiphilic bilayer membranes. In their theory individual conformations are distinguished and lateral interactions are taken into account in a Flory–Huggins approximation. Probability distributions of head, tail, and solvent segments in a bilayer are calculated in their work.

The above theories have in common that they cannot give an accurate description of the relationship between the fundamental intermolecular interactions and the static and dynamic properties of the membrane, and that they do not yield the detailed description provided by simulations. The molecular dynamics (MD) simulation method presents a way of predicting the macroscopic properties of molecular systems on the basis of atomic interactions. Nowadays, simulations of large and complex molecular systems are possible and give reliable results. Time scales of phenomena and complexity of systems that are open to investigation keep pace with ever increasing computer power.

The sodium–decanoate/decanol/water system, a lipid multibilayer system, has been thoroughly investigated as a model system for biological membranes. This system exhibits a smectic liquid–crystalline phase at room temperature, with lipid molecules arranged in bilayers. It differs from biological membranes in the type of lipids (only single chain lipids with ionic headgroups), and in the nearby presence of other bilayers, as the model system is a multibilayer system. This system has been experimentally investigated by Seelig

a) To whom correspondence is to be addressed.

 0021-9606/88/183718-15$02.10

and Niederberger by means of x-ray diffraction and NMR techniques,[8–12] leading to values of local order parameters and diffusion constants.

Previous MD simulations, mimicking this smectic liquid crystalline system, have been carried out by van der Ploeg and Berendsen.[13,14] Their simulations involved a simplification: only a single bilayer of decanol molecules was simulated, whereas head groups were treated as united atoms, held in a nearly coplanar configuration by means of a harmonic force. Our present simulation represents a far more accurate implementation of the system, and differs from the previous simulations in the following aspects:

(i) the head groups of the amphiphilic molecules are treated in full atomic detail enabling the discrimination between decanoate ions and decanol molecules;

(ii) (partial) atomic charges are included in the simulation;

(iii) aqueous degrees of freedom are explicitly treated;

(iv) sodium ions are included, constituting counterions for decanoate ions.

We are now in a position to compare results of the present simulation with those of the previous ones and with experimental results and theoretical predictions. Moreover, the structure of the lipid–water interface and properties of water in smectic systems can be studied. A preliminary report of our findings has been presented at the first EBSA Workshop.[15]

In Sec. II the method of simulation and the details of the model are described. Section III gives the results of an 80 ps simulation, performed after a preliminary simulation of a small system and after an extensive equilibration procedure. The static properties are described in Sec. III C. They include distribution functions of atoms and charges, pair correlation functions, electron density function, order parameters, and *trans–gauche* statistics. Dynamic properties are described in Sec. III D, and cover diffusion constants, *trans–gauche* transitions and reorientational correlation times. In Sec. IV the results are compared with previous simulations, with experimental data and with other theories.

II. METHOD AND MODEL

A. Method of simulation

The molecular dynamics simulation method is a procedure for the numerical integration of Newton's equations of motion. The types of forces applied in the algorithm are described in Sec. II C. A leap-frog algorithm[16] was used, which is mathematically equivalent to the algorithm of Verlet,[17] but is more efficient from a computational point of view. We used Cartesian coordinates and constrained bond lengths by the SHAKE method.[18,19] The computational unit cell contains 3166 atoms: a bilayer of 52 decanoate ions and 76 decanol molecules, and a water layer of 526 water molecules and 52 sodium ions.

Periodic boundary conditions were applied in three dimensions. A weak coupling of the system to a temperature bath at 300 K was applied.[20] Velocities of solute and solvent molecules were scaled independently, both with a coupling time constant of 0.1 ps. An isotropic pressure of 1 atm was applied to the system by weakly coupling the system to a pressure bath at 1 atm.[20] The three unit cell dimensions were scaled independently, with a coupling time constant of 0.5 ps. The integration time step was set to 2 fs. A cutoff radius for Lennard-Jones interactions of 0.75 nm was used. Coulomb interactions were treated as described in Sec. II D.

The simulation program that was used is based on GROMOS.[21] After adaptation of this program to the specific task of simulation of a membrane, a speed of 1 ps simulation (500 MD steps) per hour CPU time on a Cyber 170/760 computer was attained for the system of 3166 atoms. On a one-pipe Cyber 205 machine, a speed of 10 ps simulation per hour CPU time was realized with an extensively vectorized version of the program.

B. Composition of the model system

The composition of the system equals that of the model membrane, studied by Seelig and Niederberger[8–12] (molar ratios: sodium–decanoate: 0.41, decanol: 0.59, water: 4.11). The computational unit cell for the MD simulation contained 76 decanol molecules, 52 decanoate ions, 52 sodium ions, and 526 water molecules, leading to a total of 3166 atoms. The initial configuration of the system was derived from a hydrocarbon configuration in one of the previous simulations.[13,14] Coordinates for head group atoms of decanoate ions and decanol molecules were added, since in the previous simulations headgroups had been treated as united atoms. The water layer was generated from a liquid configuration of SPC water[22]. Randomly chosen water molecules were replaced by sodium ions.

C. Model parameters

The water model used in the simulation is the SPC model.[22] In this simple point charge model, the oxygen atom carries a charge $-0.82e$, and both hydrogen atoms carry charges of $0.41e$. The O–H bond length is 0.1 nm, the H–O–H angle is 109° 28′. As far as Lennard-Jones interactions are concerned the H_2O molecule is treated as a united atom centered on the oxygen atom. Both the bond lengths and the bond angle in SPC water are constrained by the SHAKE method.[18,19] Solute molecules are treated in full atomic detail with the exception of CH_2 and CH_3 groups, that are treated as single Lennard-Jones centers. Lennard-Jones interactions between atoms i and j have the form:

$$V(r_{ij}) = 4\epsilon_{ij}\left[(\sigma_{ij}/r_{ij})^{12} - (\sigma_{ij}/r_{ij})^{6}\right]. \quad (1)$$

Values for ϵ_{ij} and σ_{ij} were taken from GROMOS[21] and from van der Ploeg and Berendsen.[13,14] Parameters for interactions between sodium ions and water oxygens were calculated from Kistenmacher.[23] Parameters for interactions of sodium ions with other atoms follow from standard combination rules.[24] In Table I the Lennard-Jones interaction parameters are listed for all atom pairs. Bond lengths are constrained by the SHAKE method.[18,19] Equilibrium bond lengths were taken from GROMOS[21] and are given in Table II. Bond angles were treated by a harmonic potential, parameters can be found in Table III. Details on dihedral interactions are presented in Table IV. Table V, finally, summarizes

TABLE I. Lennard-Jones parameters ϵ_{ij} and σ_{ij} for atom pairs. Parameters: upper values ϵ_{ij} (kJ/mol), lower values σ_{ij} (nm).[a]

	CH_3	CH_2	C	Na	OW	OA	OM
OM	1.038	0.861	0.836	0.153	0.495	0.566	1.724
	0.313	0.313	0.297	0.295	0.327	0.316	0.263
OA	1.038	0.861	0.837	0.229	0.743	0.849	
	0.313	0.313	0.297	0.276	0.306	0.306	
OW	1.201	0.997	0.968	0.200	0.650		
	0.310	0.310	0.293	0.286	0.316		
Na	0.196	0.163	0.158	0.062			
	0.310	0.310	0.294	0.258			
C	0.504	0.418	0.406				
	0.355	0.355	0.336		OM = decanoate oxygen		
CH_2	0.518	0.430			OA = decanol oxygen		
	0.374	0.374			OW = water oxygen		
CH_3	0.624						
	0.374						

[a] Lennard-Jones interactions are excluded for nearest and next-nearest neighbors, as well as for 1–4 interactions of groups that are treated by the Ryckaert–Bellemans potential (Table IV). The hydrogen atoms of decanol and water carry partial charges, but have no Lennard-Jones parameters. These are incorporated in the parameters for OA and OW, respectively.

the (partial) charges on atoms. An interaction cutoff radius of 0.75 nm was used for Lennard-Jones and Coulomb interactions. An extra long range interaction term was calculated for Coulomb interactions (see Sec. II D). A relative dielectric constant ϵ_r of 1 was used.

D. Treatment of electrostatics

The lipid bilayer contains groups with a net charge (sodium ions and decanoate ions) and groups with dipole moments only (water molecules and decanol headgroups). Coulomb interactions are therefore expected to play an important role in the dynamics. These interactions are long ranged, so a cutoff radius as small as 0.75 nm will introduce significant errors in the dynamics. A larger cutoff radius would therefore be preferable, but that has the major drawback of a dramatical increase of the CPU time required for the simulation, as this time is proportional to the cube of the interaction cutoff radius.

We resorted to a compromise, illustrated in Fig. 1. Every tenth dynamics time step a pair list is updated, containing all charge group pairs *i–j* with $r_{ij} \leqslant 0.75$ nm. (a charge group is the smallest group of adjacent atoms, for which the sum of the atomic charges is *ne*, *n* integer). Simultaneously with the updating of this pair list, the Coulomb force is evaluated on every partially charged atom *i*, due to those atoms *j*

TABLE II. Equilibrium bond lengths (nm).

CH_3–CH_2:	0.153	
CH_2–CH_2:	0.153	
CH_2–C:	0.153	
C–OM:	0.125	
CH_2–OA:	0.143	
OA–HA:	0.100	
OW–HW:	0.100	
HW–HW:	0.163	(virtual bond length in SPC water)

TABLE III. Equilibrium bond angles and force constants: $V(\alpha) = 1/2\ k_b (\alpha - \alpha_0)^2$ (kJ/mol).

Type	k_b (kJ mol^{-1} rad^{-2})	α_0 (deg)
CH_3–CH_2–CH_2	460	111
CH_2–CH_2–CH_2	460	111
CH_2–CH_2–C	460	111
CH_2–C–OM	502	117
OM–C–OM	502	126
CH_2–CH_2–OA	460	111
CH_2–OA–HA	397	109.5

that are not in the pair list of atom *i*, but obey $x_{ij}^2 + y_{ij}^2 \leqslant R_{\text{cyl}}^2$. In the simulation we used $R_{\text{cyl}} = 1.7$ nm. One cannot go far beyond this value, due to the requirement that the interaction cutoff radius be smaller than half of the smallest unit cell dimension. As a third component, a charge distribution $\rho(z)$ is evaluated by the division of the unit cell into slices in the bilayer plane and accumulation of the charge per slice during the simulation. This process is also performed simultaneously with the updating of the pair list. A time-averaged charge distribution $\rho(z)$ is approximated by $\rho^*(z,t)$, obtained from

$$\rho^*(z,t) = \rho^*(z,t-\Delta)e^{(-\Delta/\tau)} + \rho(z,t)(1 - e^{(-\Delta/\tau)}), \quad (2)$$

where Δ is the time interval between two successive updates of the pair list, and where τ is a characteristic time, set to 0.5 ps in the simulation. The charge distribution $\rho^*(z,t)$ is the charge distribution that is present everywhere outside a cylinder with radius R_{cyl}. It represents a low-pass filter that converges to the average charge distribution $\rho(z)$, but still allows adaptation to slow changes. From this charge distribution $\rho^*(z,t)$ the field $E_z(z)$ on the axis of the cylinder can be obtained. Details are presented in the Appendix.

The total force thus results from three components:

(a) The short-range force, calculated every time step using a cutoff radius of 0.75 nm.

(b) The medium-range force, calculated every tenth time step simultaneously with the updating of the short-range pair list, and resulting from charges in a cylindrical region. This force remains active during the next ten steps.

TABLE IV. Parameters for dihedral interations. For the dihedrals CH_2–CH_2–CH_2–CH_2 and CH_2–CH_2–CH_2–CH_3 we used the Ryckaert–Bellemans potential (Refs. 40 and 41): $V(\varphi) = \Sigma_{i=0}^{5} C_i(\cos\varphi)^i$, with C_i ($i = 0,\ldots,5$): 9.28, 12.16, − 13.12, − 3.06, 26.24, and − 31.5 kJ/mol. The Ryckaert–Bellemans potential includes the interactions between first and last atom of the dihedral. For the other proper dihedrals we used: $V(\varphi) = C\cos(n\varphi + \delta)$.[a]

Type	C (kJ/mol)	n	δ (deg)
CH_2–CH_2–CH_2–OA	5.86	3	0
CH_2–CH_2–OA–HA	1.26	3	0
CH_2–CH_2–CH_2–C	5.86	3	0
CH_2–CH_2–C–OM	0.42	6	0

[a] For the improper dihedral C–OM–OM–CH_2 we used: $V(\alpha) = 167.36\ \alpha^2$ (kJ/mol).

TABLE V. Partial charges of atoms.

In decanol: OA: $-0.548e$, HA: $0.398e$, CH_2: $0.150e$
In decanoate: OM: $-0.635e$, C: $0.270e$
In water: HW: $0.410e$, OW: $-0.820e$

(c) The long-range force, resulting from the average charge distribution $\rho(z)$ outside the cylindrical region. It is sufficient to limit the source charge distribution to one double layer, because the average fields resulting from homogeneous charge distributions in adjacent layers will cancel.

This total force, in addition to bonded forces (angles, dihedrals, SHAKE) is used to update velocities every time step. For the calculation of the virial (necessary for the evaluation of the pressure components) we used forces on atoms instead of forces on molecular centers of mass, as is usually applied in pressure scaling. This was done in order to be able to incorporate the contribution to the virial from the extra-cylinder charge distribution $\rho^*(z,t)$. In practice this contribution turned out to be negligible, however. The details of this virial calculation will be reported elsewhere.

III. RESULTS

A. Simulation of a small system

Originally, a simulation was set up on a small system, with unit cell sizes of 2 (x,y) and 3.56 nm (z), consisting of 20 decanol molecules, 12 decanoate ions, 12 sodium ions, and 128 water molecules. We observed that in the course of the equilibration run this system tended towards crystallization. This is concluded from the radial distribution function for the headgroups of the lipid molecules, that shows very pronounced higher order maxima. Also, the x and y size of the unit cell changed in such a way that they obtained relative magnitudes of 2 and 3. In this way, the headgroups of decanoate ions (6 per monolayer) are able to arrange in a cubic lattice. We ascribe this crystallization to the fact that correlations in the system extend over distances comparable with the x and y unit cell dimensions. A similar observation was made in a previous simulation by van der Ploeg and Berendsen[13] on a single bilayer of 2×16 lipid molecules, where cooperativity extended over the entire unit cell. We therefore decided to increase the size of the system to 128 lipid molecules and 526 water molecules, with unit cell sizes of 4 (x,y) and 3.56 nm (z), thereby conserving the surface area of 0.25 nm^2 per head group.

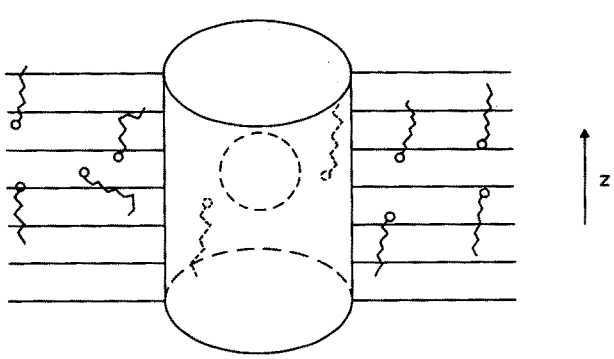

FIG. 1. Schematic representation of regions involved in the evaluation of Coulomb interactions. The z coordinate runs from the middle of one lipid bilayer to the middle of the next lipid bilayer. The radius of the sphere is 0.75 nm, the radius of the cylinder is 1.7 nm.

B. Equilibration

The initial configuration of the system was constructed by taking a hydrocarbon configuration from a simulation performed by van der Ploeg and Berendsen,[14] adding water from a liquid SPC water configuration. Randomly chosen water molecules were replaced by sodium ions. After energy minimization of the system an equilibration run was started, that was continued until such properties as potential energies, dimensions of the unit cell, and penetration depth of water into the hydrocarbon region of the membrane had more or less stabilized. It appears that the potential energy stabilizes much more quickly than the unit cell dimensions, and is therefore not a good criterion for judging whether equilibrium has been attained. The total length of the equilibration run was 100 ps. The equilibration run was started with unit cell dimensions of 4, 4, and 3.56 nm (x,y,z), corresponding to the experimental values for surface area per head group of a lipid molecule[25] of 0.25 nm^2 and thickness of lipid bilayer + water layer of 3.56 nm[8–12] After the equilibration run the unit cell sizes had stabilized on 3.87, 3.87, and 3.63 nm. This corresponds to a value for the surface area per head group of a lipid molecule of 0.234 $nm.^2$ These values still agree within experimental error with density and x-ray data. All components of the potential energy function had stabilized.

C. Static properties

1. Distribution of atom types and charges

In order to establish the structure present in the multibilayer system, the distributions of the various components in the system along the normal to the bilayer were calculated. Figure 2 displays the distributions of the head groups of decanol molecules and decanoate ions, of water molecules, and of sodium ions. The location of decanol headgroups and water molecules was taken to be determined by the position of the oxygen atoms. For decanoate headgroups the average of the two oxygen positions was taken. The distribution of the headgroups of the two lipid species is very broad. The bilayer–water interface is diffuse, while a remarkably deep penetration of water molecules into the hydrocarbon core of the lipid bilayer is observed. The distribution of sodium ions closely resembles that of water molecules, though the ion penetration into the lipid bilayer is less prominent. The decanoate headgroups preferably sit near the middle of the aqueous layer, in spite of the fact that this location involves the unfavorable exposure of part of the hydrocarbon chain to

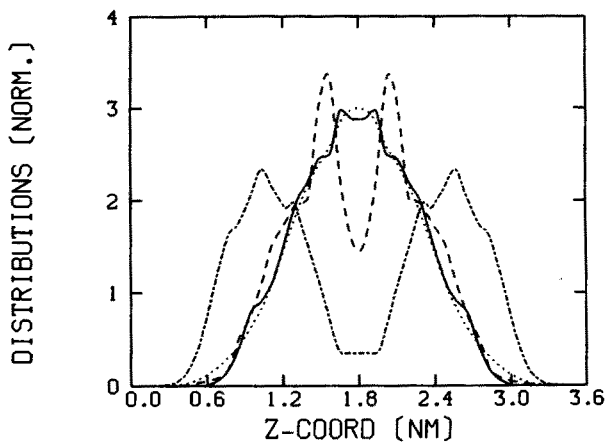

FIG. 2. Distribution of components along the normal to the bilayer, z coordinate as in Fig. 1, for head groups of decanoate ions (– –), headgroups of decanol molecules (– – – –), sodium ions (···), and water molecules (—).

a water environment. The decanol headgroups, carrying no net charge and having a relatively small permanent dipole moment, tend to be more deeply buried in the lipid layer. The overlap of sodium ion and carboxylic acid distribution suggests a membrane structure that is characterized by a charge compensation rather than by the building up of a diffuse electrical double layer as pictured in many textbooks on membranes.

In Fig. 3, a projected structure of a snapshot of the system after 30 ps simulation is given. It is evident that the layer structure has been conserved in the simulation, but the lipid head groups have a low degree of coplanarity. Though it is not visible in the two-dimensional representation, an analysis of the water–water pair correlation function in the hydrocarbon core of the membrane reveals that the water molecules in this core are never isolated but are always found in small clusters.

We investigated the occurrence of transversal waves in the membrane, because the projected structures suggest the presence of ripples in the bilayer. Fourier analysis of the 80 ps run at accessible values of the wave vector did not reveal a peak in the frequency power spectrum. This indicates that either the surface waves are highly damped or that the wave velocity is too small to be observable.

Figure 4 displays the time-averaged charge distributions along the normal to the bilayer for decanoate and sodium ions, for decanol head groups, and for water molecules. These charge distributions were calculated by assigning every (partial) atomic charge to the slice in which it is found.

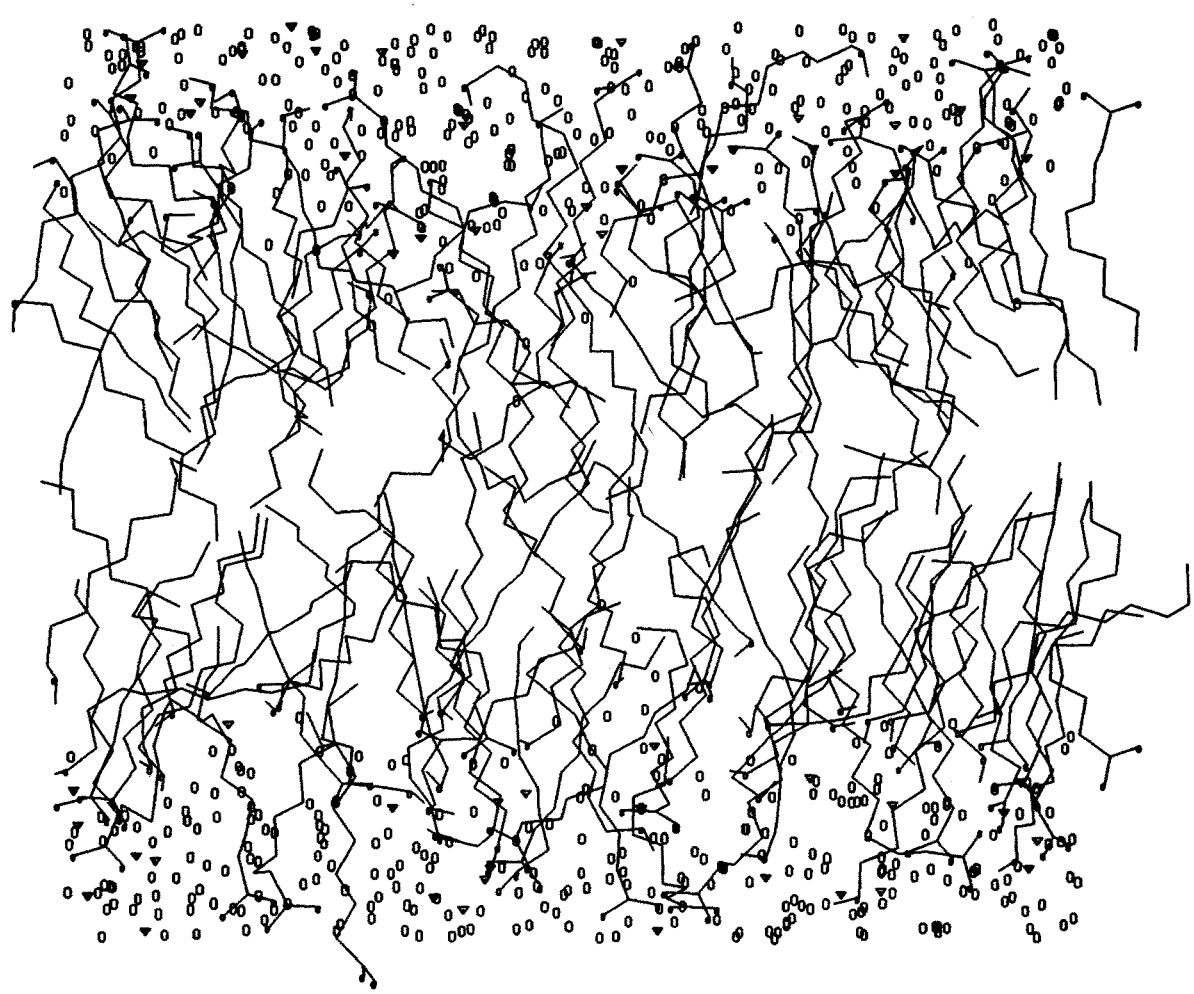

FIG. 3. Projection on the xz plane of a snapshot of the system after 30 ps simulation: decanoate ions and decanol molecules (—), sodium ions (∇), water oxygens (O), oxygens in the lipids (o).

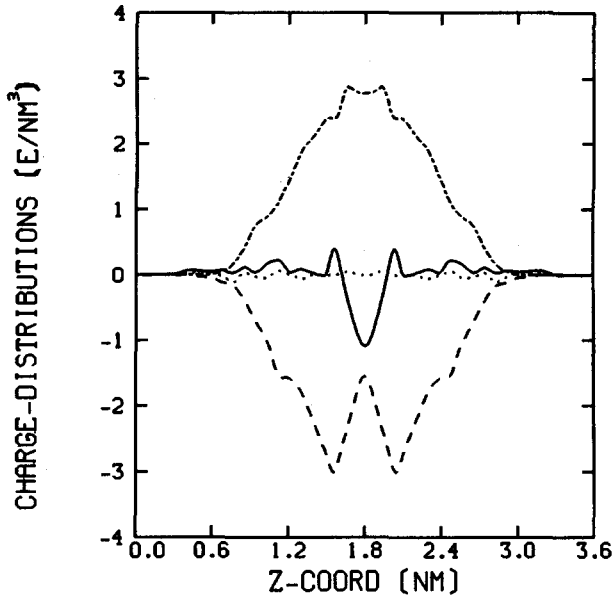

FIG. 4. Charge distributions (e/nm^3) along z of components in the system, z coordinate as in Fig. 1. Discrete (partial) atomic charges were used for the evaluation of the distributions: decanoate ions (– –), decanol molecules (···), water molecules (—), sodium ions (– – – –).

It is observed that the charge distributions of decanoate ions and sodium ions cancel to a large extent throughout the membrane. What is left of uncompensated charge is then once again largely compensated by the distribution of the dipole moments of water molecules and decanol head groups. They appear to orient in such a way that they reduce the total charge in a slice to practically zero everywhere.

An alternative way of representing charge distributions is by way of cumulative charge distributions $\rho_c(z)$, defined through $\rho_c(z) = \int_0^z \rho(z')dz'$. This is a smoother method to show the detailed charge compensation in the membrane,

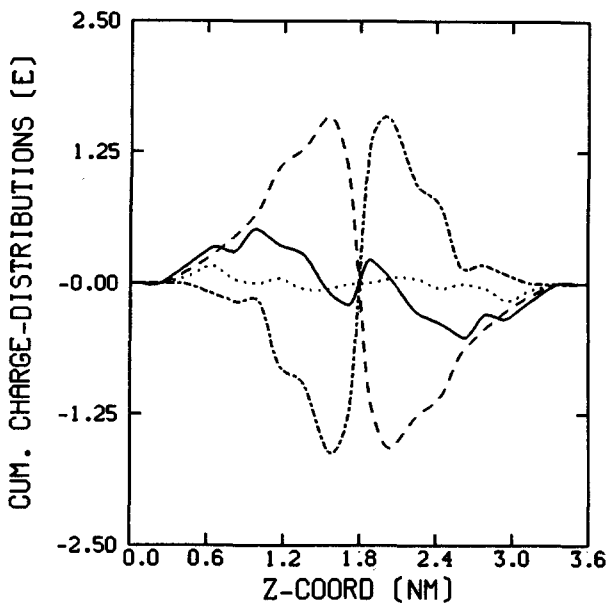

FIG. 5. Cumulative charge distributions (electronic units) of components in the system from the middle of one lipid bilayer to the middle of the next lipid bilayer: sodium + decanoate ions (– – – –), decanol molecules (···), water molecules (– – –), all components together (—).

because noise is integrated out in this way. For sodium ions and decanoate headgroups $\rho_c(z)$ integrates up to the number of electronic charges in the system, i.e., $\pm$ 52e. In Fig. 5 cumulative charge distributions are presented for sodium + decanoate, decanol, water, and for all components together. From the cumulative charge distributions for sodium + decanoate we see clearly that the decanoate ions are more on the hydrocarbon side of the interface, but it is also evident that the interface is very broad ($\approx$1 nm) and diffuse. What is left of a cumulative charge distribution after the mutual compensation of the two ion types, is most effectively compensated by the dipole moment distribution of the water molecules. The effect of the dipoles of the decanol head groups is negligible. The cumulative charge distributions practically cancel throughout the membrane. The charge distribution emerging in our simulation does not support the model of an electrical double layer with head groups confined to a sharply defined interfacial region and with a diffuse counterion distribution in the aqueous part of the system between the head groups.

2. Radial distribution functions

Pair correlation functions were calculated for various atom pairs. In Fig. 6 the pair correlation functions of sodium ions with oxygen atoms of decanoate, decanol, and water are given. These pair correlations have been corrected for the density distributions of the components in the system, i.e., for the correlation functions that would have been obtained as a result of the z distribution of the components in the system, apart from any interatomic structure. The pair correlation Na^+–OM (decanoate oxygen) exhibits a highly pronounced first neighbor peak as well as a sharp second order maximum. No correlation exists beyond this maximum. Using the location of the first minimum in the pair correlation function as a criterion for the upper bound of the existence of a bound state, one finds that 72% of the Na^+ ions is bound to at least one oxygen atom of decanoate ions. The pair correlation Na^+–OW (water oxygen) shows a pronounced first order maximum, as well as resolved second

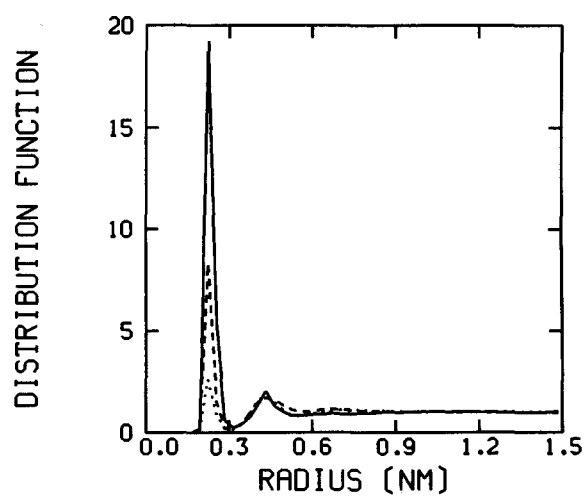

FIG. 6. Pair correlation functions of sodium ions with oxygen atoms of decanoate (OM), decanol (OA), and water (OW). sodium–OM (—), sodium–OA (···), sodium–OW (– – – –).

TABLE VI. Ligandation of sodium ions.

Number of oxygens	OM	OA	OW	Percentual occurrence
5	2	0	3	13.2
5	0	0	5	12.2
6	2	0	4	10.4
6	0	0	6	8.4
6	4	0	2	8.0
5	3	0	2	7.3
5	1	0	4	6.1
6	0	1	5	4.5
6	3	0	3	4.4
6	5	0	1	4.3
6	1	0	5	4.1
5	4	0	1	3.6
5	0	1	4	2.1
7	4	0	3	1.1

and third order neighbor peaks. As much as 98.9% of the Na^+ ions is bound to at least one H_2O molecule, applying the above criterion. OA (decanol oxygen) occurs considerably less frequent as a neighbor of Na^+ ions, as is clear from the pair correlation Na^+-OA. Only 12.5% of the Na^+ ions is liganded to decanol oxygens.

The coordination number of Na^+ to oxygen atoms is 5.5 (63.8% OW, 33.9% OM, and 2.3% OA). Both a coordination number of five and of six occur in 47% of all cases. If Na^+ ions would not distinguish between the three oxygen ligands, one would calculate, using the above coordination number, for the percentage of Na^+ ions bound to at least one OM, OW, or OA: 58.4%, 99.95%, and 46.6%. From these numbers it is clear that in the simulation Na^+ distinctly prefers ligandation to oxygens of decanoate, at the expense of water and decanol oxygens. In Table VI we list the most frequently occurring complexes of Na^+ with oxygens, with their percentual occurrence.

3. Electron density distribution

The electron density distribution in a system is a quantity that is in principle accessible to experiments. Figure 7 displays the z distribution of electrons, calculated from the MD run, and an experimental result for the electron density in a more or less similar system. No experimental data are available on the electron density in the sodium–decanoate/decanol/H_2O system. Therefore results from Levine[26] on a lecithin/water system are included in Fig. 7. A rescaling of the z repeat distance has been performed for the results of Levine, which also have an arbitrary scale on the ordinate axis.

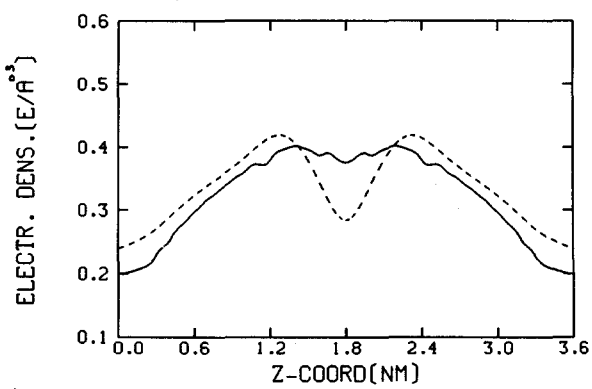

FIG. 7. Electron density distribution ($e/Å^3$) from the middle of one lipid bilayer to the middle of the next lipid bilayer, simulation (—), experiment on a dipalmitoylphosphatidylcholine/water system (rescaled) (- - -).

Though it is hazardous to compare the two curves, two comments may be made. First, the electron density falls off rapidly towards the middle of the lipid bilayer in both curves. This is generally observed in membranes and model systems for membranes. Second, the difference in electron density between headgroup region and water region that is observed experimentally, is not reproduced in our simulation. Only a small dip in the aqueous region is observed in the MD electron density function. Obviously the electronic composition of the diffuse and broad interfacial region is approximately constant.

Jönsson *et al.*[27] performed a MD simulation on a sodium–octanoate micelle in aqueous solution. They calculated the electron density in the micelle in radial direction and observed it to be less structured than is usually assumed in models used to interpret scattering data. This observation agrees with our findings and so does their conclusion that the increase in electron density from tail ends to the headgroup region is prominent, while there is no difference in the electron density between headgroup region and aqueous region.

4. Order parameters

The order parameter tensor **S** is defined by

$$S_{ij} = 1/2\ \overline{(3\cos\Theta_i \cos\Theta_j - \delta_{ij})}, \qquad (3)$$

where Θ_i is the angle between the ith molecular axis and the bilayer normal (z axis), and where the bar implies averaging over time and molecules. The molecular axes are defined per CH_2 unit. For the nth CH_2 unit we define:

z: vector from C_{n-1} to C_{n+1};

y: vector, perpendicular to z, and in the plane through C_{n-1}, C_n, and C_{n+1};

x: vector, perpendicular to z and y.

Order parameters can vary between 1 (full order along the bilayer normal) and $-1/2$ (full order perpendicular to the normal), with a value of zero in the case of isotropic orientation. From symmetry arguments, **S** is diagonal, except for S_{yz} which is usually small. The diagonal elements sum to zero, so essentially we have three independent order parameters per CH_2 unit. This number reduces to two in the case of isotropic rotation around the molecular z axis. In that case $S_{zz} = -2S_{xx} = -2S_{yy}$. S_{zz} is usually referred to as S_{chain}. Experimentally, deuterium NMR order parameters S_{CD} are available for several positions along the chain, as measured by Seelig and Niederberger.[8–12] These are defined for the direction along the CH bond and can be compared to the MD order parameters, using the relation $S_{CD} = 2/3S_{xx} + 1/3S_{yy}$. In Fig. 8 both the experimental and the MD order parameters are displayed for all CH_2 units in a chain, decanoate ions and decanol molecules treated separately. There is reasonable agreement between experimental and MD order parameters S_{CD}.

The experimentally observed plateau in the order parameters is well reproduced. The present MD order param-

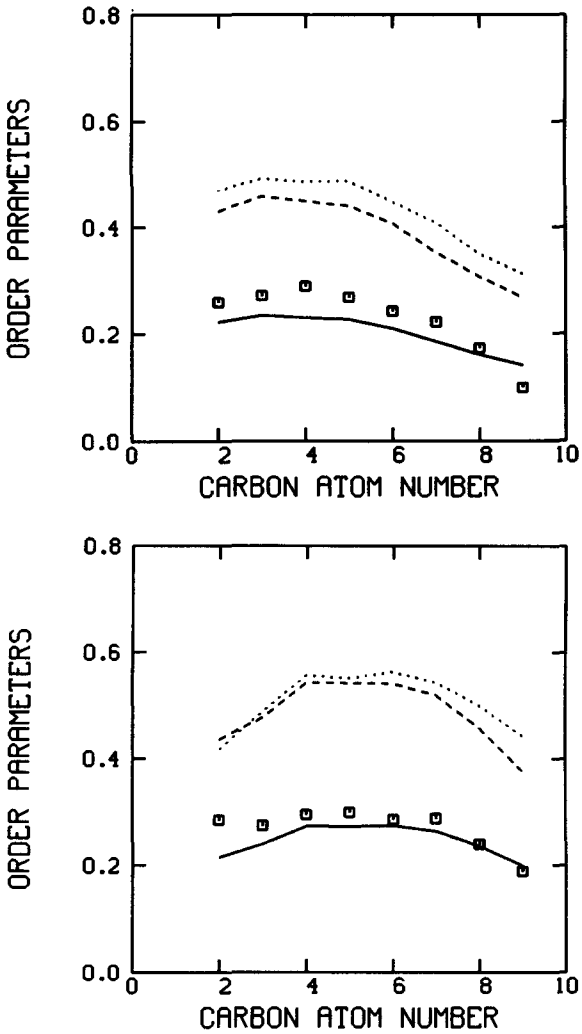

FIG. 8. Order parameters as a function of carbon atom number. Carbon atom 10 is the carbon atom of the tail CH_3 group. (a) decanol; (b) decanoate: $-S_{CD}$ (—), S_{zz} (– –), $-2S_{xx}$ (· · ·), values from experiment Refs. 8–12 (□).

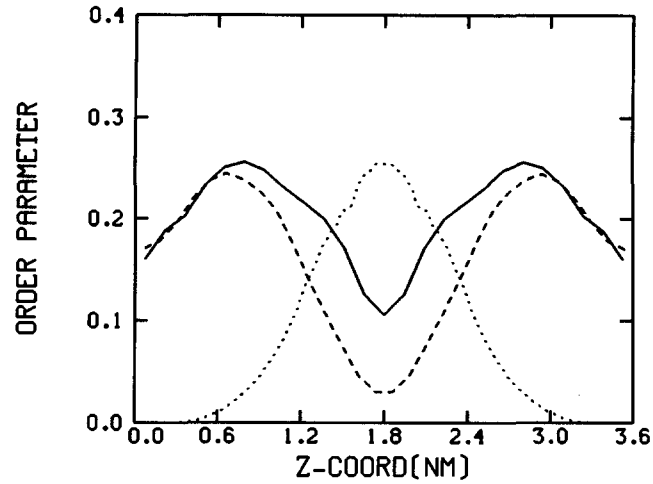

FIG. 9. Order parameters $-S_{CD}$ for decanoate + decanol chain units (—), as a function of the z coordinate of a chain unit. Z coordinate as in Fig. 1: density of CH_2 groups (arbitrary scale) (– –), density of water molecules (arbitrary scale) (· · ·).

eters tend to be somewhat lower than both the experimental ones and the ones in the previous simulations by van der Ploeg and Berendsen.[13,14] This is clearly observed for CH_2 units near the head groups of decanoate. This phenomenon reflects the fact that the lipid molecules in the present simulation aggregate in a rather loose structure, with a broad bilayer region, and accordingly a lower packing density of CH_2 groups than in the simulation by van der Ploeg and Berendsen. As is clear from Fig. 2, the head groups of the decanoate ions penetrate deeply into the aqueous layer, and it is therefore not surprising that the order parameters of CH_2 groups near these head groups will be lower. It is observed that $-2S_{xx}$ is larger than S_{zz} for all but one CH_2 unit, indicating an anisotropy of rotation around the molecular z axis. This has also been observed experimentally[28] and in the simulations by van der Ploeg and Berendsen. As an illustration of the dependence of the order parameter S_{CD} of CH_2 units on their location in the membrane, Fig. 9 displays the order parameter S_{CD} of CH_2 groups as a function of z, combined for decanol molecules and decanoate ions. The density functions of C atoms and of water molecules are included as a reference. The order parameter S_{CD} falls off towards the middle of the lipid layer, where the C atom density also decreases, and towards the middle of the aqueous layer, where water is the predominant component. These observations demonstrate the correlation of the order parameters with the packing of the hydrocarbon groups.

5. Trans–gauche statistics

The overall orientation of a molecule is one factor determining the value of the order parameter. The state of the internal dihedral angles of a molecule (g^+,t,g^-) is another one. We calculated the fraction of *trans* dihedral angles in decanoate ions and decanol molecules. These turned out to be 0.79 and 0.775, respectively. These values are in good agreement with the value of 0.79 determined by van der Ploeg and Berendsen. Applying Boltzmann statistics to the Ryckaert–Bellemans potential for dihedral interactions (*trans–gauche* energy difference: 2.9288 kJ/mol) and excluding adjacent *gauche* conformations of opposite sign[29] one calculates a value of 0.66 for the fraction of *trans* dihedral angles. Therefore, the effective *trans–gauche* energy difference in the simulation is higher than the Ryckaert–Bellemans value, and amounts to 4.25 kJ/mol. Clearly, the structure that is present in the membrane prefers *trans* configurations. We calculated the fraction of *trans* dihedral angles as a function of the angle of the central bond of a dihedral with the normal to the bilayer. In accordance with the observations of van der Ploeg and Berendsen,[13,14] it is observed that dihedral rotations (g^+,g^-) occur preferably around bonds that are parallel to the normal.

In Fig. 10, we display the fraction of *trans* dihedral angles vs the dihedral number, separately for decanoate and decanol. Dihedral number one is the dihedral between carbon atoms two and three, counting downwards from the head group. An odd–even effect is observed, that is most prominent for decanoate. The explanation for the observed opposite polarity in this phenomenon for decanoate and decanol is found in the behavior of the head groups. From symmetry arguments the average dipole vector of the head

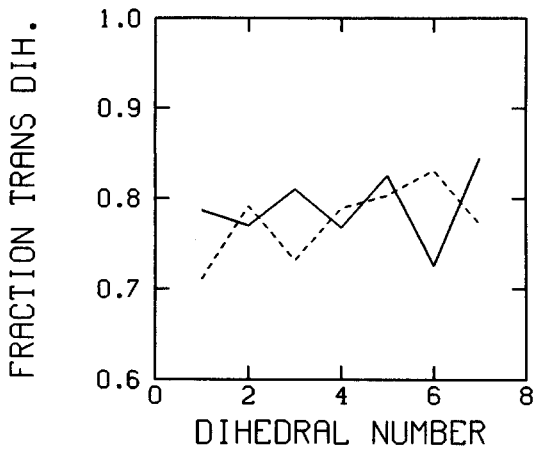

FIG. 10. Fraction of *trans* dihedral angles as a function of the dihedral number. Dihedral number one is the dihedral closest to the headgroup: decanoate ions (—), decanol molecules (– –).

groups of the lipids will orient along the normal to the bilayer. This implies that the CH_2–C bond in decanoate will on average be oriented along the normal to the bilayer. The next CH_2–CH_2 bond will therefore point away from the director, and the first dihedral in decanoate will thus have a relatively large fraction of *trans* dihedral angles, as dihedral rotations (g^+,g^-) occur preferably around bonds that are parallel with the normal to the bilayer. For decanol it is the CH_2–O bond that is an average parallel with the normal to the bilayer, and the first dihedral will thus have a larger fraction of *gauche* dihedral angles.

In Fig. 11 the fraction of *trans* dihedral angles is displayed as a function of the z coordinate of the central bond of a dihedral. The density function of carbon atoms is also included in this figure. It is observed that the two curves are isomorphic: the fraction of *trans* dihedral angles is high where the density of carbon atoms is high and falls off where this density function falls off.

The occurrence of g^+tg^- or g^-tg^+ configurations is infrequent. The average number of these so-called kinks per decanoate ion or per decanol molecule is 0.14, respectively, 0.20, where van der Ploeg and Berendsen calculated a number of 0.20 for the lipids in their simulation. The fraction of

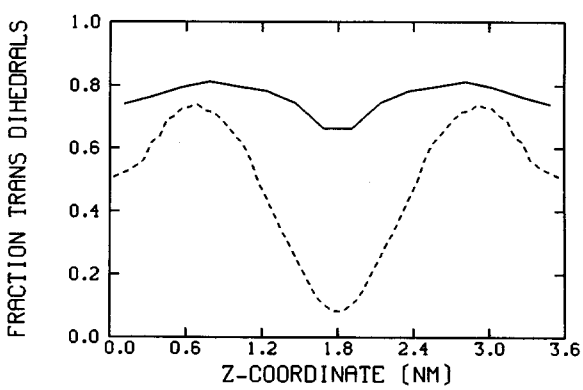

FIG. 11. Fraction of *trans* dihedral angles as a function of the z coordinate of the central bond of a dihedral, combined for decanoate and decanol (—). Z coordinate as in Fig. 1. Density of carbon atoms (arbitrary scale) (– – –).

kinks observed in the present simulation is far too low to support the kink model[30] for the explanation of the plateau in the order parameters, which requires at least one kink per lipid molecule. Statistically one would expect numbers of 0.182 and 0.199, making use of the fraction of *trans* angles calculated in the simulation, assuming a random distribution of *gauche* dihedrals, and excluding g^+g^- and g^-g^+ sequences. The fraction of kinks per decanoate ion observed in the simulation is even smaller than expected statistically. This implies that the distribution of *gauche* dihedral angles in decanoate ions is nonrandom, in agreement with the observed odd–even effect in decanoate. The observation that decanoate ions exhibit slightly less *gauche* rotations than decanol molecules, together with the observed odd–even effect is reflected in the smaller number of kinks per decanoate ion.

D. Dynamic properties

1. Trans–gauche dynamics

A dihedral transition is considered to have taken place whenever the crossing of a barrier in the dihedral potential is followed by the crossing of the corresponding (local) minimum in the dihedral potential.[31] Using this definition, which avoids the counting of a temporary transgression of the barrier as a true transition, we calculated the mean time between two transitions of the same dihedral. For decanoate ions this time is 30.7 ps, for decanol molecules it is 31.3 ps, with errors of $\pm$ 0.5 ps. The two types of lipids have the same dihedral transition rate, which is however 2.5 times lower than in the previous simulations,[13,14] where a value of 12.3 ps was calculated for the mean time between transitions of the same dihedral. The corresponding value in the micelle simulation by Jönsson *et al.*[28] is 16.0 ps. We can think of two reasons for the low transition rate in the present simulation. In the first place there are the dominant electrostatic interactions, that may well reduce the flexibility of the chains near the charged head groups. A change in the internal configuration of a molecule can be prohibited by the strong intermolecular Coulomb interactions. We calculated the dihedral transition rate as a function of the z coordinate of the central bond of a dihedral. It is observed that the dihedral transition rate is lower by a factor of 2 in the aqueous part of the system than in the hydrocarbon core, where electrostatic interactions play a less important role, and where dihedrals are on average separated by several CH_2 units from the charged head groups. We expect that this effect is only of secondary importance however, because the density of dihedrals in the aqueous region of the system is low. In the second place, the greater flexibility of the chains in the z direction, as compared to the previous simulation, is expected to reduce the transition rate.

2. Diffusion constants

Lateral diffusion constants were calculated for Na^+ ions, and for the centers of mass of decanoate ions, decanol molecules, and water molecules, from mean squared displacements, using the relation:

$$\lim_{t\to\infty} \langle r^2(t) \rangle = 4Dt, \tag{4}$$

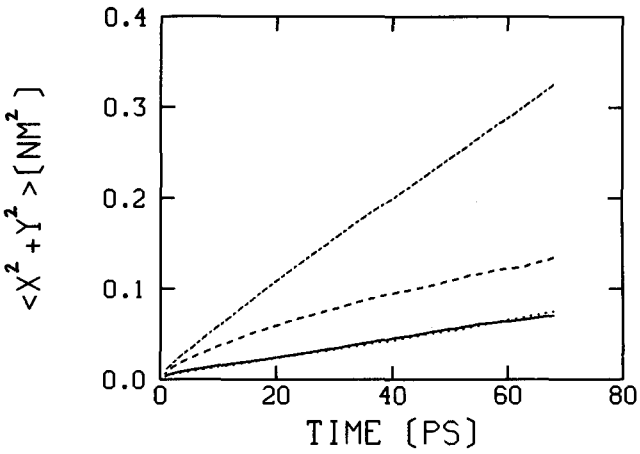

FIG. 12. Average squared lateral displacements as a function of time for the centers of mass of water molecules (- - - -), decanol molecules (– –), decanoate ions (—), and sodium ions (···).

where $r^2(t) = [x(t) - x(0)]^2 + y(t) - y(0)]^2$.

In Fig. 12 the mean squared lateral displacements of the four components are given as a function of time. From Eq. (4) one calculates for the diffusion constants:

sodium: $D = (2.7 \pm 0.3) \times 10^{-6}$ cm^2 s^{-1};
decanoate: $D = (2.7 \pm 0.3) \times 10^{-6}$ cm^2 s^{-1};
decanol: $D = (5.2 \pm 0.4) \times 10^{-6}$ cm^2 s^{-1};
water: $D = (1.2 \pm 0.05) \times 10^{-5}$cm^2 s^{-1}.

The values of the diffusion constants of the lipid molecules are in reasonable agreement with the value of 1.5×10^{-6} cm^2 s^{-1}, measured by Seelig[12] with the use of a nitroxide spin label. In the simulation by van der Ploeg and Berendsen, a value of 1.1×10^{-5} cm^2 s^{-1} was calculated for the diffusion constants of the lipids. We note that the discrepancy of one order of magnitude between experimental and MD results in the previous simulations, with simplified treatment of head groups, has disappeared in the present simulation. Hence we conclude that the mechanism determining the diffusion constants of the lipid molecules is the hydrodynamic interaction of the headgroups with the aqueous layer, rather than interactions within the layer.

The diffusion constant of H_2O is a factor of 3 smaller than the one in the pure SPC model (3.6×10^{-5} cm^2 s^{-1}). Water in the membrane diffuses three times slower than bulk water, so not only are the lipids slowed down by the presence of H_2O, but also is the water motion affected by the presence of the lipids. A similar observation was made in NMR experiments on a similar soap–water system,[32] indicating that the state of water in models of biological systems is different from that of ordinary bulk water. We can compare the diffusion constants of H_2O in our simulation with experimental results on a potassium–palmitate/water system. Callaghan *et al.*[33] determined a lateral diffusion constant of H_2O in a 70:30 w/w potassium–palmitate/D_2O system at 65 °C of 0.85×10^{-5} cm^2 s^{-1}. Using the temperature dependence of the diffusion constant of SPC water, one arrives at a value of 0.52×10^{-5} cm^2 s^{-1} at 300 K for the diffusion constant of H_2O in their system. Ukleja and Dohane,[34] for the same sytem at 75 °C, measured a value of 1.6×10^{-5} cm^2 s^{-1}, which can be extrapolated to a value at 300 K of 0.77×10^{-5} cm^2 s^{-1}. The correspondence between MD and experimental values is encouraging. The difference of a factor of 2 may be caused by the fact that the diffusion of decanol and decanoate is expected to be faster than that of palmitate, and by the fact that SPC water diffuses faster than real water.

We investigated the dependence of the diffusion constant of water molecules on their location within the system. Therefore, the system was subdivided into four parts and the lateral diffusion constants of water in these parts were determined:

1° $0.0 < z < 0.7$ nm, middle of lipid bilayer: $D = (5.0 \pm 1.0) \times 10^{-6}$ cm^2 s^{-1};
2° $0.7 < z < 1.2$ nm, headgroups of decanol: $D = (6.5 \pm 1.0) \times 10^{-6}$ cm^2 s^{-1};
3° $1.2 < z < 1.6$ nm, headgroups of decanoate: $D = (1.0 \pm 05) \times 10^{-5}$ cm^2 s^{-1};
4° $1.6 < z < 1.8$ nm, middle of water layer: $D = (1.2 \pm .05) \times 10^{-5}$ cm^2 s^{-1}.

From these data it is evident that the diffusion of water in the lipid part of the bilayer is slower than in the aqueous part of the system. In the lipid region of the membrane the diffusion of H_2O is not much faster than that of decanol molecules, the main constituents of the interior of the lipid bilayer.

3. Reorientational correlation times

Reorientational correlation times were calculated for three molecular H_2O vectors. The vectors used are:

(a) the dipole vector;
(b) the vector connecting the hydrogen atoms;
(c) the vector, perpendicular to (a) and (b).

Autocorrelation functions were evaluated for the Legendre polynomials $P_1(\cos\Theta) = \cos\Theta$, and $P_2(\cos\Theta) = 3/2\cos^2\Theta - 1/2$, where $\Theta_i(t)$ is the angle between $\mathbf{n}_i(t')$ and $\mathbf{n}_i(t'+t)$, and $\mathbf{n}_i$ are the three molecular H_2O vectors. In Fig. 13, the autocorrelation functions of $P_1(\cos\Theta)$ for the three molecular H_2O vectors are displayed. We calculated time constants assuming a single exponential decay in the region from 1 to 10 ps. In Table VII the time constants are listed as calculated in our simulation, in the water simulation by Postma,[35] and in the water simulation by Teleman.[36] The conclusion is that the rotational motion of water for all three molecular axes is considerably slowed down in our membrane compared to pure SPC water. This is in sharp contrast with the conclusion drawn by Jönsson *et al.*[28] in their simulation of a sodium–octanoate micelle in aqueous solution. They state that both the rotational and the translational motion of water molecules are not significantly affected by the presence of the micelle. In our simulation, both the translational and the rotational motion of water molecules are clearly slowed down compared to bulk water. Though one may argue that in our simulation the density of ionic components is higher by a factor of 2.5, this does not seem to give a sufficient explanation for the observed discrepancy.

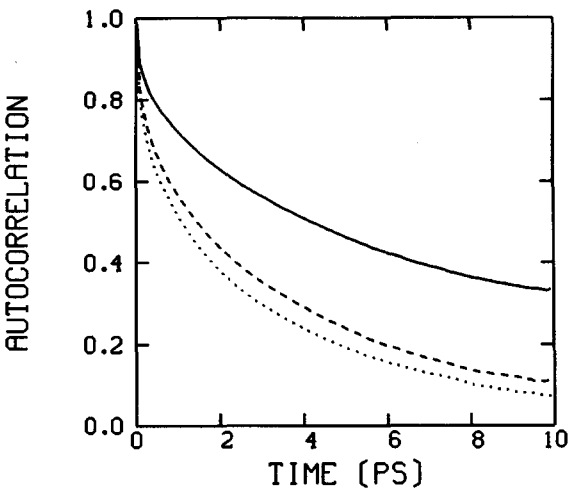

FIG. 13. Reorientational correlation function P_1 (cos Θ) as a function of time for three molecular vectors of H_2O: dipole vector (—), H–H vector (- - -), vector normal to the H–O–H plane (···).

The values of $\tau_{1,a}$ and $\tau_{2,a}$ in our simulation differ most from the corresponding values for SPC water. This implies that it is the rotation of the water dipole vector that is inhibited most in the membrane. The water dipoles tend to line up in the direction of the field caused by the solute charges, as we have seen before. This field will not drift significantly in a time span of a few ps, which explains the large values of $\tau_{1,a}$ and $\tau_{2,a}$. A rotation of one of the other axes does not necessarily involve rotation of the dipole vector, and these rotations are accordingly less hindered. From a free diffusion model one expects a ratio of $\tau_{1,a}$ over $\tau_{2,a}$ of 3. This relationship is already violated for pure SPC water, where the ratio is 2.4. For water in the membrane the ratio is only 2.1, which is another indication of the hindered rotation of water in the lipid/water system.

We investigated the dependence of $\tau_{2,a}$ on the z coordinate of a water molecule. Three regions were discerned:

middle of lipid bilayer : $\tau_{2,a} = 6.7$ ps;
headgroup region : $\tau_{2,a} = 4.5$ ps;
aqueous region : $\tau_{2,a} = 3.6$ ps.

Water molecules that penetrated the hydrocarbon core of the lipid bilayer not only diffuse slower (see Sec. III D 2), but also rotate slower than their counterparts in the aqueous region.

TABLE VII. Time constants of rotational autocorrelation functions for water molecules.

	This work	Postma	Teleman
$\tau_{1,a}$ [a,c]	8.8 ps	3.5 ps	3.1 ps
$\tau_{1,b}$	4.6 ps	3.1 ps	2.7 ps
$\tau_{1,c}$	3.9 ps	···	2.0 ps
$\tau_{2,a}$ [b,c]	4.1 ps	1.5 ps	1.3 ps
$\tau_{2,b}$	3.9 ps	1.8 ps	1.7 ps
$\tau_{2,c}$	3.6 ps	···	1.0 ps

[a] τ_1: first order spherical harmonic functions.
[b] τ_2: second order spherical harmonic functions.
[c] a, b, c refer to dipole vector, H–H vector, and normal to HOH plane, respectively.

IV. DISCUSSION

A. Comparison with experimental data

When comparing the values of order parameters and diffusion constants in the present and the previous simulations[13,14] with experimental data, the conclusion must be that the present modeling of the model membrane is more successful in the prediction of dynamical variables, but slightly less successful in the prediction of static properties of the model membrane than the previous simulations. This is not surprising when we realize that on the one hand, the present model is much closer to the experimental conditions, but on the other hand, we are now faced with the evaluation of Coulomb forces in an ionic system. This makes high demands on the properties of the water model that is used, and on the parameters for the evaluation of the interactions between (fully or partially) charged components. As we have seen, the values of diffusion constants in the present simulation have been considerably brought down compared to the previous simulations and are now much closer to the experimental ones, though still somewhat higher. The explicit presence of water molecules together with the detailed description of the head groups of lipid molecules introduces a hydrodynamic damping term that is responsible for the lower values of the diffusion constants.

The presence of water molecules not only influences the lateral motion of the lipid molecules, it also distorts the high degree of coplanarity of the head groups of the lipids. Whereas in the previous simulations the head groups of the lipids were confined to a relatively narrow region by means of a harmonic force exerted on them, the presence of the water molecules now creates a broad and very diffuse lipid–water interface. Obviously, the forces at the interface do not produce a sharp boundary. It is this vertical spread of the head groups that reduces the packing density of the hydrocarbon tails of the lipids, resulting in lower values of the order parameters than in the previous simulations. The overall picture emerging from our simulation is that of a disordered lipid structure with substantial water penetration and almost complete overlap of the distributions of negative lipid charges and positive counterions, and is contrary to the generally accepted picture of the diffuse electrical double layer. One should bear in mind however, that the lipids in our simulation have only one, relatively short, chain and that the charge density in the system is high, thereby differing from the situation in real biological systems.

B. Distribution functions compared with other theories

In order to illustrate the spread of the hydrocarbon chain units in the present simulation, Fig. 14 gives the z distribution of carbon atoms in the present simulation, in the simulation by van der Ploeg and Berendsen,[14] and in the model of Gruen.[6] It is clear that the distribution of C atoms in the present simulation is much broader, due to the fact that the headgroups of the lipids are free to move. The density of carbon atoms in the lipid region is lower than in the

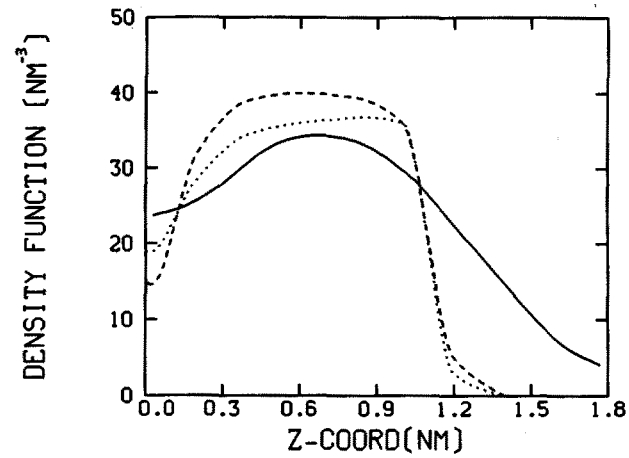

FIG. 14. Distribution function of carbon atoms (nm^{-3}) as a function of z. The z coordinate runs from the middle of the lipid layer to the middle of the aqueous layer. Present simulation (—), simulation by van der Ploeg and Berendsen, Ref. 14 (- - -), model of Gruen, Ref.6 (···).

other models, except for the very middle of the lipid bilayer, where the dip in the density is less pronounced. The lower density of carbon atoms explains the lower value of the order parameters in our simulation.

In the work of Leermakers *et al.*[7] the z distributions of several chain units were calculated. These distributions can be compared with the MD distributions, by making the middle of the bilayer and the mean positions of the head groups coincide for the two systems. In Fig. 15 the z distributions of the tail methyl group and the CH_2 group next to the head group are presented for the model of Leermakers and for our simulation. Only chain units from one monolayer were counted. There is good agreement between the curves in the two systems. The MD curves show approximately the same width throughout the membrane, whereas the distributions in the model of Leermakers tend to sharpen up towards the head group region. The half-widths of the MD distributions are approximately 1 nm, showing the large spread of the

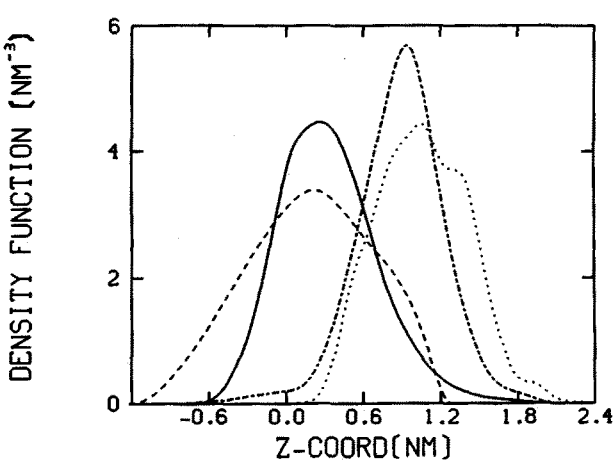

FIG. 15. Distribution of carbon atoms (nm^{-3}) as a function of z coordinate. $z = 0$ corresponds to the middle of the lipid bilayer, $z = 1.8$ nm to the middle of the aqueous layer. MD result for CH_3 groups (—), result of Leermakers, Ref. 7, for CH_3 groups (- - -), MD result for carbon atom 9 (counted from CH_3 group) (···), result of Leermakers for carbon atom 9 (- - - -).

components along z. The agreement between the models is somewhat artificial though, because the large spread of the MD distributions is caused, among others, by the different behavior of the two types of lipids present in our simulation. Our distributions would considerably narrow on considering only one type of lipid. It would be interesting to see how the distributions of Leermakers would change after refinement of headgroup representation in their model.

C. Distribution of counterions

Jönsson *et al.*[37] developed a model for the distribution of counterions in the aqueous region between two negatively charged bilayer sheets. They solved the Poisson–Boltzmann equation to find the charge distribution $\rho(z)$ of counterions in a medium with relative dielectric constant ϵ_r between two sheets with a negative surface charge density σ, that are a distance $2b$ apart. Their solution reads

$$\rho(z) = \frac{(\epsilon_0 \epsilon_r kTs^2/eb^2)}{\cos^2(sz/b)}, \qquad |z| < b,$$
$$\rho(z) = 0, \qquad |z| \geq b, \tag{5}$$

where s is the solution of $s \tan s = \sigma eb/(2\epsilon_0 \epsilon_r kT)$.

Both the solution given by Eq. (5), filling in constants from our system, and the charge distribution of Na^+ ions from the simulation are displayed in Fig. 16. The two distributions are in no way compatible. The reasons for this discrepancy are in the implicit restrictions in the model of Jönsson: the negative charges are restricted to planar surfaces and counterions and dielectricum are confined to the region in between these surfaces. Such a model can obviously not be used for charged membrane systems.

D. Penetration of water

The penetration of water into the hydrocarbon core of the membrane is deeper than is usually assumed for biological membranes, though not much is really known about the behavior of water in these membranes. The water distribution in our system can be compared to the distributions found in the micelle simulation of Jönsson[27] and in the lattice model of Leermakers *et al.*[7] The lipid chains in the model of

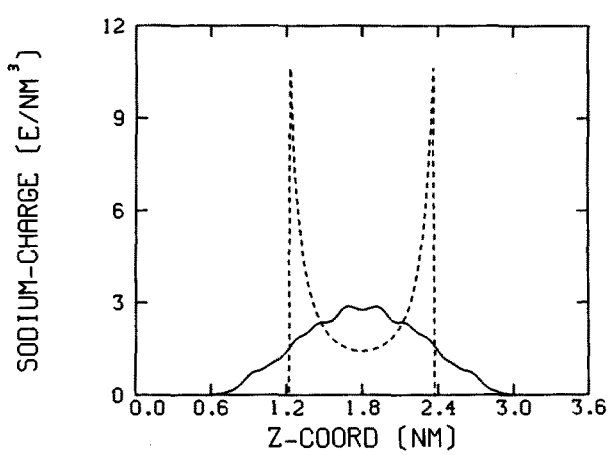

FIG 16. Charge distribution of sodium atoms as a function of z, z as in Fig. 1. Simulation (—), model of Jönsson, Ref. 37 (- - -).

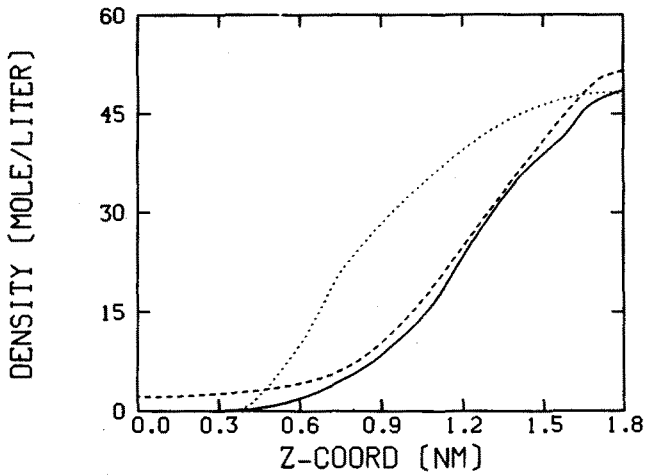

FIG. 17. Density function of water molecules (mol per liter) from the middle of lipid bilayer to the middle of the aqueous region. MD (—), model of Leermakers, Ref. 7 (- - -), model of Jönsson, Ref. 30 (···).

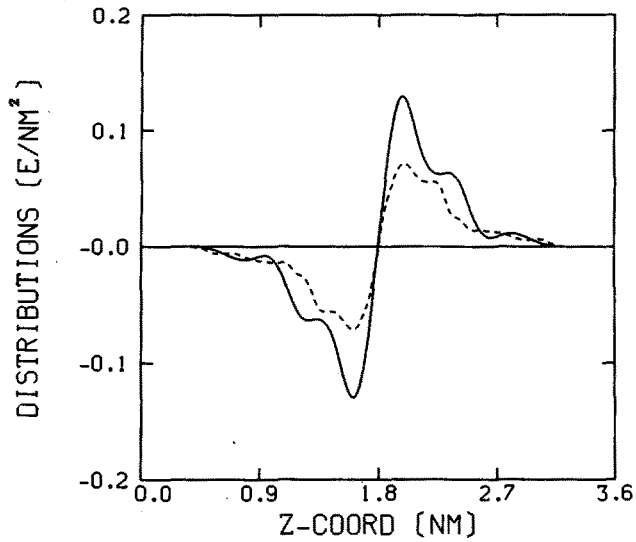

FIG. 18. Distributions (e/nm^2) from the middle of one lipid bilayer to the middle of the next lipid bilayer. Cumulative charge distribution of sodium + decanoate (—), z polarization of water molecules (- -).

Jönsson are two units shorter than the ones in our simulation, so in order to compare the water distributions we proceeded by making the average positions of the headgroups of the lipids coincide. In Fig. 17 the distribution of water molecules in the three systems (in mole per liter) are displayed. Except for the nonzero penetration of water in the middle of the bilayer in their model, the results from Leermakers agree remarkably well with our results. The density of water in the micelle is substantially higher than in our bilayer, but the penetration depths are equal. The densities of water in the aqueous region in the MD simulations is lower than the bulk water density because of the nonzero contributions of other components. In all three systems the water penetration is substantial, whereas the interface extends over about 1 nm.

E. Charge compensation and dielectric behavior

One of the outstanding features of the simulation is the almost complete charge compensation throughout the system. On the one hand, the reason for this compensation is found in the fact that, on average, as much as 72% of the Na^+ ions are bound to decanoate head groups. On the other hand, it should be realized that it costs free energy to maintain an overall charge density, with its concomitant long-range electric field, and a molecular system will tend to minimize the average charge density as long as this is not counteracted by other sources of free energy. In addition the water polarization very effectively neutralizes any remaining charge density (see Fig. 5). It is of interest to analyze to what extent this inhomogeneous system behaves as a continuous dielectric medium by comparing the average dipole density or polarization $\mathbf{P}$ (produced by water molecules; the alcoholic dipoles can be ignored) with the average field caused by the solute charge density ρ_0. In a medium with dielectric constant $\epsilon = \epsilon_0\epsilon_r$ the polarization $\mathbf{P}$ is proportional to the electric field $\mathbf{E}$:

$$\mathbf{P} = \epsilon_0\chi\mathbf{E}, \tag{6}$$

where $\chi = \epsilon_r - 1$ is the dielectric susceptibility of the medium. The divergence of $\mathbf{P}$ represents a charge density ρ_w induced by the polarization:

$$\text{div}\,\mathbf{P} = -\rho_w. \tag{7}$$

The total charge density $\rho_{\text{tot}} = \rho_0 + \rho_w$ relates to $\mathbf{E}$ as

$$\text{div}\,\mathbf{E} = \rho_{\text{tot}}/\epsilon_0 \tag{8}$$

which, with Eqs. (6) and (7) yields

$$\text{div}\,\mathbf{P} = (1 - 1/\epsilon_r)\rho_0. \tag{9}$$

This means that the induced charge density $-$ div $\mathbf{P}$ practically compensates the solute charge density ρ_0 for media with a high dielectric constant. Instead of Eq. (9) we can consider the integrated form:

$$\mathbf{P}(z) = (1 - 1/\epsilon_r)\int_0^z \rho_0(z')dz'. \tag{10}$$

The integral on the right-hand side represents the time-averaged cumulative charge distribution of the solute charges, which for a homogeneous dielectric medium is proportional to the electric field:

$$\mathbf{E}_z(z) = 1/\epsilon \int_0^z \rho(z')dz'. \tag{11}$$

The z component of the water polarization as a function of z can be calculated by summing per slice in the bilayer the z components of the dipole vectors of those water molecules that have their oxygen atom in the slice. In Fig. 18 both the water polarization and the cumulative solute charge distributions are given. The two curves have a similar form. This leads one to the proposition that the average water polarization in the system is imposed by the field caused by the solute charge distribution.

It is tempting to derive the effective dielectric constant from the extent to which the cumulative solute charge distribution is compensated by the water polarization [Fig. 18 and Eq. (10)]. This yields a value for ϵ of less than 3! The discrepancy with Fig. 5 is apparent. When the charge density due to the water molecules is directly evaluated from the water charges, as has been done in Fig. 5, the compensation is complete, indicating a very high dielectric constant. The

reason for this discrepancy is that Eq. (7) is incomplete: the induced charge density is not only due to the first derivative of the dipole density, but also to the second derivative of the quadrupole density and higher derivatives of higher multipoles. These terms cannot be disregarded in systems where gradients occur over molecular distances. The dielectric constant, being an expression of dipolar behavior, loses its significance in such systems.

When we correct the polarization of water for the density function of water in the system, we obtain the time-averaged z component of the dipole moment p_z of a water molecule as a function of z. Except for the middle of the aqueous layer, where p_z is approximately zero, p_z has a relatively constant value throughout the membrane, that is approximately 5% of the physical dipole moment of a water molecule. Hence, there is no saturation of the dielectric medium. The distribution of the water molecules is such that compensation of the electric field due to the solute charges does not require a highly varying value of p_z in the membrane.

F. Effects of insufficient shielding

SPC water does not possess polarizability, and owes its dielectric properties solely to its permanent dipole moment. The value of ϵ_r, for SPC water is not exactly known. It was estimated by Jönsson *et al.*[27] to be as low as 20, although a recent evaluation[38] indicates a value of 82. The high frequency value of 1 is in any case smaller than the value of 5 of real water. It is therefore questionable whether SPC water can sufficiently shield the ions, that are abundant in the system. Insufficient shielding of the Na^+ ions can lead to condensation of these ions on the decanoate head groups, which in turn reduces the repulsion between the head groups, resulting in a smaller surface area per head group of a lipid molecule.

Jönsson, *et al.*[27] investigated the effect of charge reduction in their simulation of a sodium–octanoate micelle in aqueous solution. On reducing all charges to half their original values, which effectively increases the relative dielectric constant of the solvent to four, which is close to the high frequency dielectric constant of real water, they observed a substantially sharper water–hydrocarbon interface. A simulation of the sodium–decanoate/decanol/H_2O system with sodium and decanoate charges reduced to half their original values has just been completed by us. Results will be reported separately. From a physical standpoint it is clear however, that a refinement of the water model is the fundamental improvement to be made. We therefore conclude that the introduction of polarizability into standard MD is a matter of great urgency.[39]

ACKNOWLEDGMENTS

This work was supported by the Foundation for Biophysics, under the auspices of the Netherlands Organization for Pure Research, ZWO. The simulations were carried out on the Cyber 170/760 computer of the Computer Center of the University of Groningen.

APPENDIX: TREATMENT OF LONG-RANGE FORCES

The force on atom i at time t is given by

$$\mathbf{F}_i(t) = \mathbf{F}_i^s(t) + \mathbf{F}_i^l(t), \tag{A1}$$

where

$$\mathbf{F}_i^s(t) = \sum_j \mathbf{F}_{ij}(t), \text{ for all } j \text{ with } r_{ij}(0) \leqslant R_{\text{cutoff}}, \tag{A2}$$

and where $t = 0$ is the time of updating the pair list,

$$\mathbf{F}_i^l(t) = q_i \sum_j q_j \frac{\mathbf{r}_i(t) - \mathbf{r}_j(t)}{4\pi\epsilon_0 r_{ij}(t)^3},$$

$$\text{for all } j \text{ with } r_{ij}(0) \geqslant R_{\text{cutoff}} \tag{A3}$$

assuming that only Coulomb forces contribute for $r_{ij} \geqslant R_{\text{cutoff}}$.

On the assumption that $\mathbf{r}_i$ and $\mathbf{r}_j$ are constant during 10 steps, $\mathbf{F}_i^l(t)$ is given by

$$\mathbf{F}_i^l(t) = q_i \mathbf{R}_i, \text{ independent of } t, \tag{A4}$$

where $\mathbf{R}_i$ is given by

$$\mathbf{R}_i = \sum_{\substack{j \neq i \\ r_{ij}(0) > R_c}} \frac{q_j \mathbf{r}_{ij}(0)}{4\pi\epsilon_0 r_{ij}(0)^3}. \tag{A5}$$

As pointed out previously, $\mathbf{F}_i^l(t)$ is evaluated by means of a summation over a cylindrical region, and is updated every 10th time step, i.e., every 0.02 ps. The regions over which the long-range forces are evaluated are displayed in Fig. 1. A time-averaged charge distribution $\rho^*(z)$ is supposed to be present everywhere outside a cylinder. For reasons of symmetry, the electric field on the cylinder axis due to the distribution only has a z component, that is given by

$$E_z(z) = -\int_{R_{\text{cyl}}}^{\infty} 2\pi r\, dr \int_{-\infty}^{\infty} \frac{dz' \rho^*(z')(z'-z)}{[r^2 + (z'-z)^2]^{3/2}}, \tag{A6}$$

with $\rho^*(z') = 0$ for $z' \leqslant 0$ and for $z' \geqslant$ Box (3), being the unit cell dimension along z.
We have

$$\int_{R_{\text{cyl}}}^{\infty} \frac{r\, dr}{(r^2 + a^2)^{3/2}} = (R_{\text{cyl}}^2 + a^2)^{-1/2},$$

so that

$$E_z(z) = -2\pi \int_{-\infty}^{\infty} \frac{\rho^*(z')(z'-z)dz'}{[R_{\text{cyl}}^2 + (z'-z)^2]^{1/2}}. \tag{A7}$$

From this field, evaluated through numerical integration, the forces on charged atoms and the contribution to the potential energy are readily found.

[1] J. F. Nagle, J. Chem. Phys. **63**, 1255 (1975).
[2] J. F. Nagle, J. Membr. Biol. **27**, 233 (1976).
[3] F. W. Wiegel and A. J. Kox, Adv. Chem. Phys. **41**, 195 (1980).
[4] F. Jähnig, J. Chem. Phys. **70**, 3279 (1979).
[5] F. Marcelja, Bioch. Bioph. Acta **367**, 165 (1974).
[6] D. W. R. Gruen, J. Phys. Chem. **89**, 146, 153 (1985).
[7] F. A. M. Leermakers, J. M. H. M. Scheutjens, and J. Lyklema, Bioph. Chem. **18**, 353 (1983)
[8] J. Seelig and W. Niederberger, Biochemistry **13**, 1585 (1974).
[9] W. Niederberger and J. Seelig, Ber. Bunsenges. Phys. Chem. **78**, 974 (1974).
[10] J. Seelig, Q. Rev. Biophys. **10**, 353 (1979).

[11]J. Seelig, J. Am. Chem. Soc. **92**, 3881 (1970).
[12]J. Seelig, J. Chem. Phys. **59**, 841 (1973); **61**, 2946 (1974).
[13]P. van der Ploeg and H. J. C. Berendsen, J. Chem. Phys. **76**, 3271 (1982)
[14]P. van der Ploeg and H. J. C. Berendsen, Mol. Phys. **11**, 1 (1983).
[15]H. J. C. Berendsen and E. Egberts, in *Structure, Dynamics and Function of Biomolecules, First EBSA Workshoe, Saltsjöbaden*, edited by A. Ehrenberg, R. Rigler, A. Gräslund, and L. Nilsson (Springer, Berlin, 1986), p. 275.
[16]R. W. Hockney and J. W. Eastwood, *Computer Simulation Using Particles* (McGraw–Hill, New York, 1981).
[17]L. Verlet, Phys. Rev. **159**, 98 (1967).
[18]W. F. van Gunsteren and H. J. C. Berendsen, Mol. Phys. **34**, 1311 (1977).
[19]J. P. Ryckaert, G. Ciccotti, and H. J. C. Berendsen, J. Comp. Phys. **25**, 327 (1977).
[20]H. J. C. Berendsen, J. P. M. Postma, W. F. van Gunsteren, A. Dinola, and J. R. Haak, J. Chem. Phys. **81**, 3684 (1984).
[21]GROMOS: Groningen Molecular Simulation is a software package developed by W. F. van Gunsteren and H. J. C. Berendsen, University of Groningen, 1987.
[22]H J C. Berendsen, J. P. M. Postma, W. F. van Gunsteren, and J. Hermans, in *Intermolecular Forces*, edited by B. Pullman (Reidel, Dordrecht, 1981), p. 331.
[23]H. Kistenmacher, H. Popkie, and E. Clementi, J. Chem. Phys. **58**, 1689 (1973).
[24]P. K. Warme and H. A. Scheraga, J. Comp. Phys. **12**, 49 (1973).
[25]B. Gallot and A. Skoulios, Kolloid Z. u. Z. Polymere **208**, 37 (1966).
[26]Y. K. Levine, A. Bailey, and M. H. F. Wilkins, Nature **220**, 577 (1968).
[27]B. Jönsson, O. Edholm, and O. Teleman, J. Chem. Phys. **85**, 2259 (1986).
[28]G. Stulen, Thesis, University of Groningen, 1977.
[29]O. Edholm, H. J. C. Berendsen, and P. van der Ploeg, Mol. Phys. **48**, 379 (1983).
[30]H. J. Träuble, J. Membr. Biol. **4**, 193 (1973).
[31]E. Helfand, J. Chem. Phys. **69**, 1010 (1978).
[32]J. Charvolin and P. Rigny, Chem. Phys. Lett. **18**, 515 (1973).
[33]P. T. Callaghan, M. A. Le Gros, and D. N. Pinder, J. Chem. Phys. **79**, 6372 (1983).
[34]P. Ukleja and J. W. Doane, in *Ordering Two Dimensions*, edited by P. Sinha (Elsevier, New York, 1980), p. 427.
[35]J. Postma, Thesis, University of Groningen, 1985.
[36]O. Teleman, Thesis, University of Lund, 1986.
[37]B. Jönsson, H. Wennerström, and B. Halle, J. Phys. Chem. **84**, 2179 (1980).
[38]J. Anderson, J. J. Ullo, and S. Yip, J. Chem. Phys. **87**, 1726 (1987).
[39]J. R. Grigera, H. J. C. Berendsen, and T. P. Straatsma, J. Phys. Chem. **91**, 6269 (1987).
[40]J. P. Ryckaert and A. Bellemans, Faraday Discuss. Chem. Soc. **66**, 95 (1978).
[41]J. P. Ryckaert and A. Bellemans, Chem. Phys. Lett. **30**, 123 (1975).